ACS APPLIED MATERIALS & INTERFACES

Research Article

www.acsami.org

Nanotopographical Manipulation of Focal Adhesion Formation for Enhanced Differentiation of Human Neural Stem Cells

Kisuk Yang,[†,‡] Kyuhwan Jung,[§] Eunkyung Ko,[†] Jin Kim,[†] Kook In Park,[∥] Jinseok Kim,*[,§] and Seung-Woo Cho*[,†]

[†]Department of Biotechnology and [‡]Department of Biomaterials Science and Engineering, Yonsei University, Seoul 120-749, Republic of Korea

[§]Center for Bionics, Korea Institute of Science and Technology, Seoul 136-791, Republic of Korea

[∥]Department of Pediatrics and BK21 Project for Medical Sciences, Yonsei University College of Medicine, Seoul 120-752, Republic of Korea

ABSTRACT: Manipulating neural stem cell (NSC) fate is of great importance for improving the therapeutic efficacy of NSCs to treat neurodegenerative disorders. Biophysical cues, in addition to biochemical factors, regulate NSC phenotype and function. In this study, we assessed the extent to which surface nanotopography of culture substrates modulates human NSC (hNSC) differentiation. Fibronectin-coated polymer substrates with diverse nanoscale shapes (groove and pillar) and dimensions (ranging from 300 to 1500 nm groove width and pillar gap) were used to investigate the effects of topographical cues on hNSC morphology, alignment, focal adhesion, and differentiation. The majority of nanopatterned substrates induced substantial changes in cellular morphology and alignment along the patterned shapes, leading to alterations in focal adhesion and F-actin reorganization. Certain types of nanopatterned substrates, in particular the ones with small nanostructures (e.g., 300−300 nm groove ridges and 300−300 nm pillar diameter gaps), were found to effectively enhance focal adhesion complex development. Consequently, these substrates enhanced hNSC differentiation toward neurons and astrocytes. Nanotopographical-induced formation of focal adhesions in hNSCs activates integrin-mediated mechanotransduction and intracellular signaling pathways such as MEK-ERK, which may ultimately promote gene expression related to NSC differentiation. This strategy of manipulating matrix surface topography could be applied to develop culture substrates and tissue engineered scaffolds that improve the efficacy of NSC therapeutics.

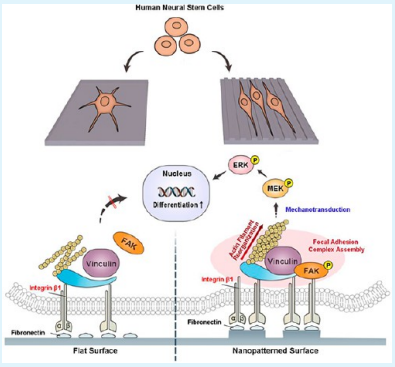

KEYWORDS: *nanotopography, human neural stem cells, focal adhesion, mechanotransduction, differentiation*

1. INTRODUCTION

Manipulating stem cell fate is important for successful therapeutic application of stem cells. Various factors, soluble and insoluble, have been shown to control stem cell fate by generating biochemical and biophysical signals.[1] Recent research has focused on biophysical cues provided by extracellular matrices (ECMs; e.g., topography, stiffness, and elasticity) that regulate stem cell phenotype and function.[1−6] More specifically, surface topography has been shown to modulate stem cell proliferation and differentiation by altering intracellular signal transduction and gene expression.[7−11] By engineering culture substrate surface topography to provide more favorable microenvironments that enhance stem cell proliferation or direct differentiation, we may be able to improve the efficacy of stem cell therapies.

Micro- or nanoscale surface topography promotes and facilitates self-renewal, proliferation, and lineage-specific differentiation of stem cells. Specifically, McMurray et al. reported that nanoscale-patterned polymer surfaces support long-term maintenance of the undifferentiated phenotype and multipotency of mesenchymal stem cells.[12] In addition, nanopatterned polymer substrates have been show to promote self-renewal of embryonic stem cells (ESCs).[13] Studies have also elucidated the topographical effects of aligned micro- and nanostructures on stem cell differentiation. Aligned groove nanopatterned polymer substrates significantly enhance neuronal differentiation of human mesenchymal stem cells (hMSCs)[14] and human ESCs (hESCs).[15] Béduer et al. demonstrated that human neural stem cells (hNSCs) grown on groove micropatterned surfaces exhibited highly organized neurite outgrowth along the aligned patterns, indicating enhanced neuronal differentiation.[16] Topographical cues generated by specific scales of submicro- or nanopatterns significantly promote osteogenic differentiation of hMSCs.[17]

Alterations to stem cell focal adhesions may explain the effects of surface topography on stem cell behavior.[9,18] Surface topography typically facilitates integrin clustering and focal adhesion assembly in stem cells, which induces cytoskeleton

Received: June 4, 2013
Accepted: July 30, 2013
Published: July 30, 2013

reorganization and alters cytoskeletal tension.[1,19] The mechanical tension altered by topography stimulates nuclear mechanotransduction via nucleus reorganization, which rearranges the centromere through deformation of the nucleus.[20,21] These changes alter gene expression involved in stem cell proliferation and differentiation, and ultimately affect stem cell phenotype and function.[1]

Despite accumulating evidence that suggests surface topography effects on stem cell behavior through focal adhesions, the majority of studies test patterned substrates containing only a single type of geometry and dimension. In fact, the molecular mechanism responsible for topographical manipulation of stem cell proliferation and differentiation is not known. Identifying specific surface topographies that promote focal adhesion of stem cells is important for designing functional culture substrates and tissue engineered scaffolds that maximize the efficacy of stem cell therapeutics. To do this, we must examine the effects of nanopatterned substrates with a wide variety of dimensions and geometries concomitant with investigations into the molecular mechanisms responsible for surface topography promotion of stem cell proliferation and differentiation.

In this study, we demonstrate that nanotopography can manipulate focal adhesion and promote differentiation of hNSCs. Nanopatterns with differing shapes (groove and pillar) and dimensions (300 nm increases within the range of 300−1500 nm) were tested to promote focal adhesion and enhance differentiation of hNSCs. Expression and organization of representative focal adhesion assembly and mechanosensitive proteins (focal adhesion kinase (FAK) and vinculin) were examined in hNSCs cultured on nanoscale groove and pillar patterned surfaces. We determined that the size of nanopattern structures (groove width and pillar gap) is critical for promoting cellular alignment, focal adhesion formation, and differentiation of hNSCs. Nanoscale groove and pillar patterns at specific dimensions and geometries that facilitate focal adhesion formation were found to efficiently induce differentiation of hNSCs into neuronal and astrocyte lineages. Because hNSCs possess the potential to differentiate into neuronal and glial lineages,[22,23] nanotopographical manipulation of hNSC differentiation could be used to develop functional stem cell therapeutics for the treatment of neurodegenerative diseases.

2. MATERIALS AND METHODS

2.1. Fabrication of Nanopatterned Substrates. Nanopatterned polyurethane acrylate (PUA) substrates were fabricated by nanoimprinting. Briefly, we poured PUA solution (Ebecryl 265, SK-UCB Co., Ulsan, Korea) onto a silicon master (produced by fabrication technology) and covered it with a polyethylene terephthalate (PET) film (SH82, SUNCHEM, Gyeongsan, Korea). The PUA was cured by exposure to ultraviolet (UV) ray (22.5 W/cm^2) for 30 s. The PET film containing the PUA pattern was carefully peeled off from the silicon master and further exposed to UV for 12 h. The prepared patterns were cleaned by soaking in 70% ethanol for 1 h and treatment with O_2 plasma for 30 s. The patterns were cleaned once more with 70% ethanol for 1 h prior to surface coating of fibronectin, a major ECM protein, by immersion in a fibronectin solution (10 μg/mL, Sigma, St. Louis, MO) for 2 h. Surface coating of fibronectin was performed to facilitate adhesion of cells to the pattern surface.

2.2. Culture of hNSCs. hNSCs were derived from the telencephalon (HFT13) as previously described.[24] The cells were plated at a density of 6.0 × 10^6 cells/ml and cultured in Dulbecco's modified Eagle's medium/Nutrient Mixture F-12 (DMEM/F12) medium (Gibco, Gaithersburg, MD) supplemented with basic fibroblast growth factor (bFGF) (20 ng/mL, Sigma), leukemia inhibitory factor (LIF) (10 ng/mL, Sigma), and N-2 supplement (Gibco) in humidified air with 5% CO_2 at 37 °C. These conditions induce hNSC growth as neurospheres.

2.3. Differentiation of hNSCs on Nanopatterned Substrates. hNSCs that dissociated from the neurospheres were seeded onto nanopatterned PUA substrates and cultured at a density of 3.0 × 10^5 cells/mL. To induce spontaneous differentiation, hNSCs were maintained in DMEM/F12 medium without supplementation of mitogenic factors bFGF and LIF. Flat PUA substrates were used as a negative control. The PUA substrates were coated with 10 μg/mL fibronectin to facilitate adhesion of hNSCs. After 5 days in culture, hNSC differentiation was analyzed by immunocytochemical staining and quantitative real-time polymerase chain reaction (qRT-PCR).

2.4. Immunocytochemistry. Immunocytochemistry for hNSC staining was performed as previously described.[24] In brief, hNSCs cultured on the nanopatterned substrates were fixed with 4% (w/v) paraformaldehyde (Sigma) for 15 min and permeabilized with 0.1% (v/v) Triton X-100 (Sigma) for 5 min. After blocking with 2% (v/v) goat serum (sigma) for 45 min, the cells were incubated with primary antibodies at 4 °C overnight. The following primary antibodies were used for staining: rabbit polyclonal anti-nestin (1:200; Abcam, Cambridge, U.K.), mouse monoclonal anti-neuronal class III β-tubulin (Tuj1) (1:100; Millipore, Temecula, CA), and mouse monoclonal anti-glial fibrillary acidic protein (GFAP) (1:200; Millipore). After washing with phosphate buffered saline (PBS), secondary antibodies Alexa Fluor-488 goat anti-mouse IgG (1:500) and Alexa Fluor-594 donkey anti-rabbit IgG (1:500) (Invitrogen, Carlsbad, CA) were added and incubated for 45 min. Cell nuclei were counterstained with 4′,6-diamidino-2-phenylindole (DAPI, Sigma). Antibody binding was observed under a fluorescent microscope (Carl Zeiss, Jena, Germany) or confocal microscope (LSM 700, Carl Zeiss).

2.5. qRT-PCR. Total RNA for qRT-PCR assay was prepared by using an RNeasy Mini kit (Qiagen, Chatsworth, CA, USA) for each sample (n = 3 per group) according to the manufacturer's instructions. RNA concentration was determined by measuring absorbance of the samples at 260 nm using a spectrophotometer. Reverse transcription for preparing cDNA from RNA samples was performed with 5 ng of pure total RNA using the SuperScript III First-Strand Synthesis System (Invitrogen). qRT-PCR was performed using a StepOnePlus Real-Time PCR System (Applied Biosystems, Foster City, CA) as previously described.[24] TaqMan Fast Universal PCR Master Mix (Applied Biosystems) was used for the reaction. The hNSC gene expression profiles were quantified with TaqMan Gene Expression Assays (Applied Biosystems) for each target (nestin, Hs00707120_s1; Tuj1, Hs00801390_s1; GFAP, Hs00909238_g1; FAK, Hs01056457_m1; vinculin, Hs00419715_m1; and glyceraldehyde 3-phosphate dehydrogenase (GAPDH), Hs02758991_g1). The expression level of target genes was determined by the comparative C_t method, whereby the target is normalized to the endogenous reference (GAPDH).[25] The relative expression of each marker in hNSCs cultured on nanopatterned substrates was normalized to that of hNSCs cultured on flat substrates.

2.6. Scanning Electron Microscopy (SEM). The morphology and shape of cells adhering to the patterned substrates were observed by SEM hNSCs on the patterned substrates were fixed with 4% paraformaldehyde for 1 h and rinsed with PBS three times. The samples were dehydrated with a graded ethanol series (50%, 70%, 80%, 90%, and 100% for 10 min each) and dried. The dried samples were mounted on aluminum stub and sputter-coated with platinum. SEM (FEI XL 30 ESEM, Philips, Eindhoven, Netherlands) was used to image the samples.

2.7. Focal Adhesion Staining. hNSCs were stained for the filamentous actin (F-actin), vinculin, and the nucleus using the Actin Cytoskeleton and Focal Adhesion Staining Kit (FAK100) (Millipore) according to the manufacturer's instructions. The stained factors were observed under a fluorescent microscope (Carl Zeiss).

2.8. Western Blot. Total protein was extracted from hNSCs grown on flat or nanopatterned substrates using a lysis buffer (pH 7.4) containing 25 mM Tris base, 0.4 M sodium chloride, 0.5% (w/v)

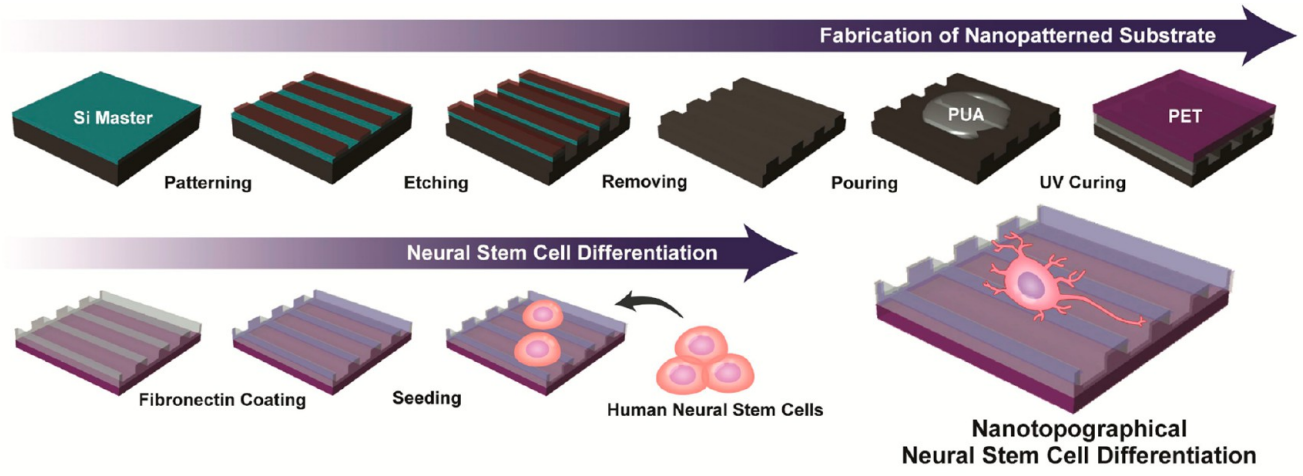

Figure 1. Nanopatterned polymer substrates were fabricated to promote hNSC differentiation.

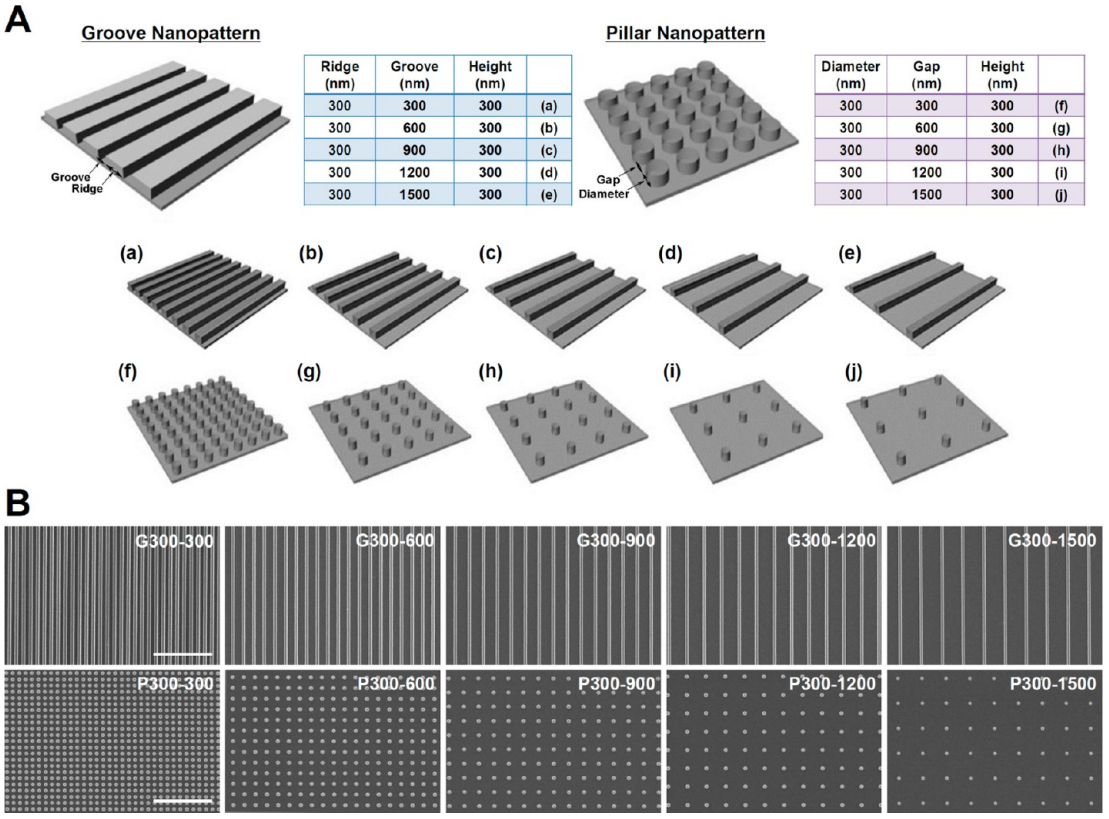

Ridge (nm)	Groove (nm)	Height (nm)	
300	300	300	(a)
300	600	300	(b)
300	900	300	(c)
300	1200	300	(d)
300	1500	300	(e)

Diameter (nm)	Gap (nm)	Height (nm)	
300	300	300	(f)
300	600	300	(g)
300	900	300	(h)
300	1200	300	(i)
300	1500	300	(j)

Figure 2. Surface characterization of the nanopatterned PUA substrates revealed (A) nanoscale ridge/groove and pillar patterned arrays with groove sizes and pillar gap ranges from 300 to 1500 nm. (B) SEM was used to image the patterned arrays, scale bars = 5 μm.

sodium dodecyl sulfate, and a protease inhibitor cocktail (Sigma). Total protein concentrations in each sample were determined by BCA assay kit (Thermo Scientific, Waltham, MA). The proteins in each sample were separated by 10% sodium dodecyl sulfate polyacrylamide gel electrophoresis and transferred to polyvinylidene fluoride membranes (Millipore). The membranes were blocked with 5% nonfat skim milk for 1 h at room temperature and incubated overnight with primary antibodies at 4 °C. The following primary antibodies were used: rabbit polyclonal anti-FAK[pY^{397}] (1:1000; Invitrogen) and rabbit monoclonal anti-β-actin (1:2500; Cell Signaling, Beverly, MA). The signals for target proteins were detected by using an enhanced chemiluminescence kit (GE Healthcare, Buckinghamshire, U.K.) according to the manufacturer's instructions.

2.9. Adhesion and Signal Transduction Inhibition Assay. hNSCs were seeded on flat or nanopatterned substrates in DMEM/F12 medium. To inhibit cell adhesion, the hNSCs were treated with 25 μM U0126 (ERK1/2 inhibitor, Cell Signaling) or anti-integrin β1 (1:40; Millipore). One day after treatment, F-actin and cell nuclei were stained with phalloidin-Alexa Fluor 488 (1:200; Invitrogen) and DAPI (Sigma), respectively. Stained structures were observed under a fluorescent microscope. The expression of focal adhesion proteins (vinculin and FAK) and differentiation markers (Tuj1 and GFAP) in cells treated with U0126 and anti-integrin β1 was quantified by qRT-PCR and compared to the untreated flat surface group.

2.10. Statistical Analysis. Quantitative data are expressed as mean ± standard deviation. Statistical analyses were performed using an

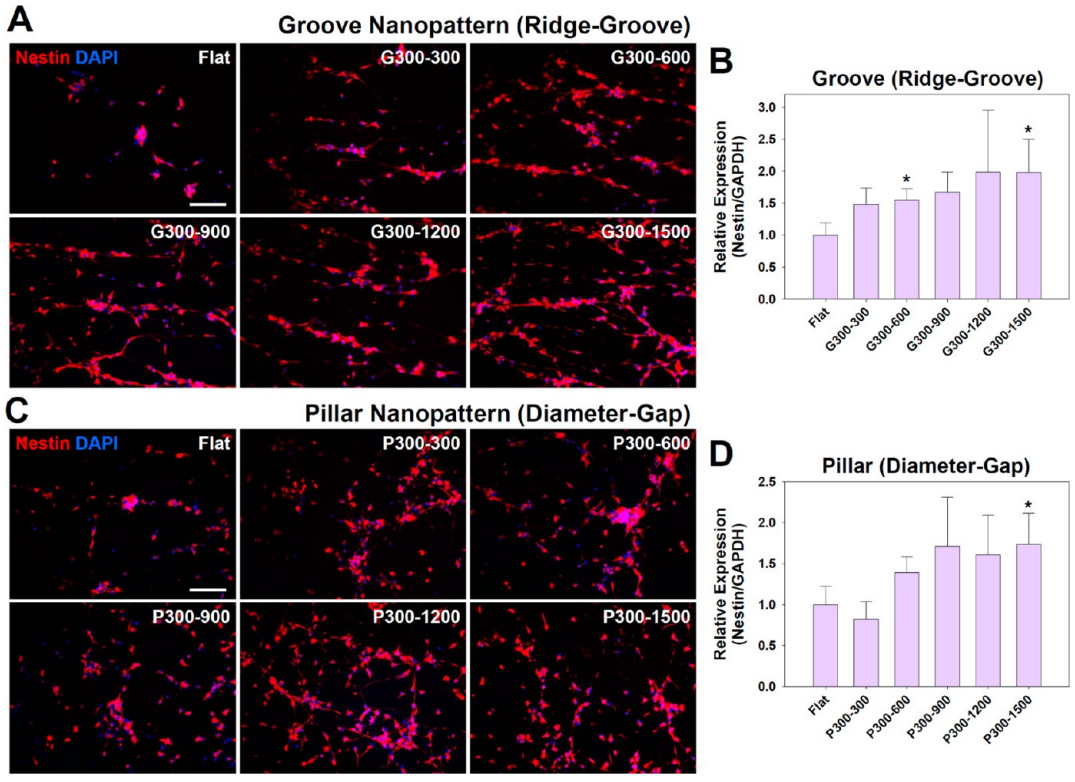

Figure 3. Expression of the undifferentiated NSC marker nestin is shown for hNSCs grown on nanopatterned polymer substrates for 5 days. Immunocytochemical staining of nestin revealed nestin-expressing cells aligned in response to (A) groove and (C) pillar nanopatterns, scale bars = 100 μm. qRT-PCR was used to measure nestin gene expression in hNSCs grown on (B) groove and (D) pillar nanopatterns. Data are expressed as mean ± standard deviation (n = 3, *p < 0.05, compared to the flat surface group).

unpaired Student's t test with Sigma-Plot software (Systat Software Inc., Chicago, IL) as previously described.[26] Values of p < 0.01 or 0.05 were considered statistically significant.

3. RESULTS AND DISCUSSION

3.1. Fabrication of Nanopatterned Polymer Substrates. Nanopatterned polymer substrates with diverse geometries and sizes were prepared to examine the nanotopographical effects of culture substrates on adhesion, spreading, and differentiation of hNSCs. Nanoscale groove and pillar patterned arrays were fabricated on PET substrates using UV-assisted capillary force lithography (Figure 1). A PUA solution was poured and cured onto the PET substrates by exposure to UV light (Figure 1). The sizes of the grooves in the resulting patterns (ridge, 300 nm; height, 300 nm) ranged from 300 to 1500 nm (increased by 300 nm) (Figure 2A). The gaps in the pillar patterns (diameter, 300 nm; height, 300 nm) also ranged from 300 to 1500 nm (increased by 300 nm; Figure 2A). SEM analysis showed highly uniform groove and pillar nanostructure patterns on the fabricated substrates (Figure 2B). The nanopatterned PUA substrates were coated with the ECM protein fibronectin to facilitate hNSC adhesion.

PUA can provide several advantages for producing the substrates with nanostructured features. PUA can be easily cured by UV exposure. In addition, photocured PUA possesses more favorable mechanical properties for nanopattern fabrication compared with polymers typically used for micropatterned substrate and microfluidic device fabrication (e.g., polydimethylsiloxane; PDMS).[27] Because PUA is more rigid, elastic and exhibits better impact strength than PDMS, a PUA replica can be easily peeled off from the silicon master without significant compromises in flexibility while retaining nanopatterned structures.[27] Therefore, PUA can replicate efficiently and accurately the nanopatterns of the silicon master mold. This process is quite simple, inexpensive, and suitable for reproducible and scalable production of nanostructured features.[28] Considering that the fidelity of nanopatterned structures is critical for regulating stem cell behavior, PUA can provide an efficient material platform for nanopatterned substrate fabrication for stem cell experiments.

Stem cells or progenitors are usually exposed to diverse biophysical cues from surrounding microenvironments including topographical stimulation during development and tissue repair process. Architectural complexities of ECM structures with isotropic and anisotropic features can provide stem cells with distinct topographies in nano- to microscale dimensions.[29] Several studies have described that nanopattern shapes and dimensions modulate differentiation of stem cells. Thus, we selected anisotropic groove and isotropic pillar nanopatterns with the ranges of 300−1500 nm to mimic the topographical cues produced by ECM structures of native tissue for hNSC differentiation.

3.2. Alignment of hNSCs on the Nanopatterned Substrates. hNSCs were seeded onto the fabricated nanopatterned PUA substrates and cultured in the absence of mitogenic growth factors, bFGF and LIF. NSCs undergo spontaneous differentiation under culture conditions without supplementation of mitogenic factors[24] and growth factors that induce neuronal or glial differentiation of hNSCs were not used in this study. Immunofluorescent staining of the undifferentiated NSC marker nestin revealed that hNSCs aligned in response to the pattern shapes (Figure 3A and C). In addition,

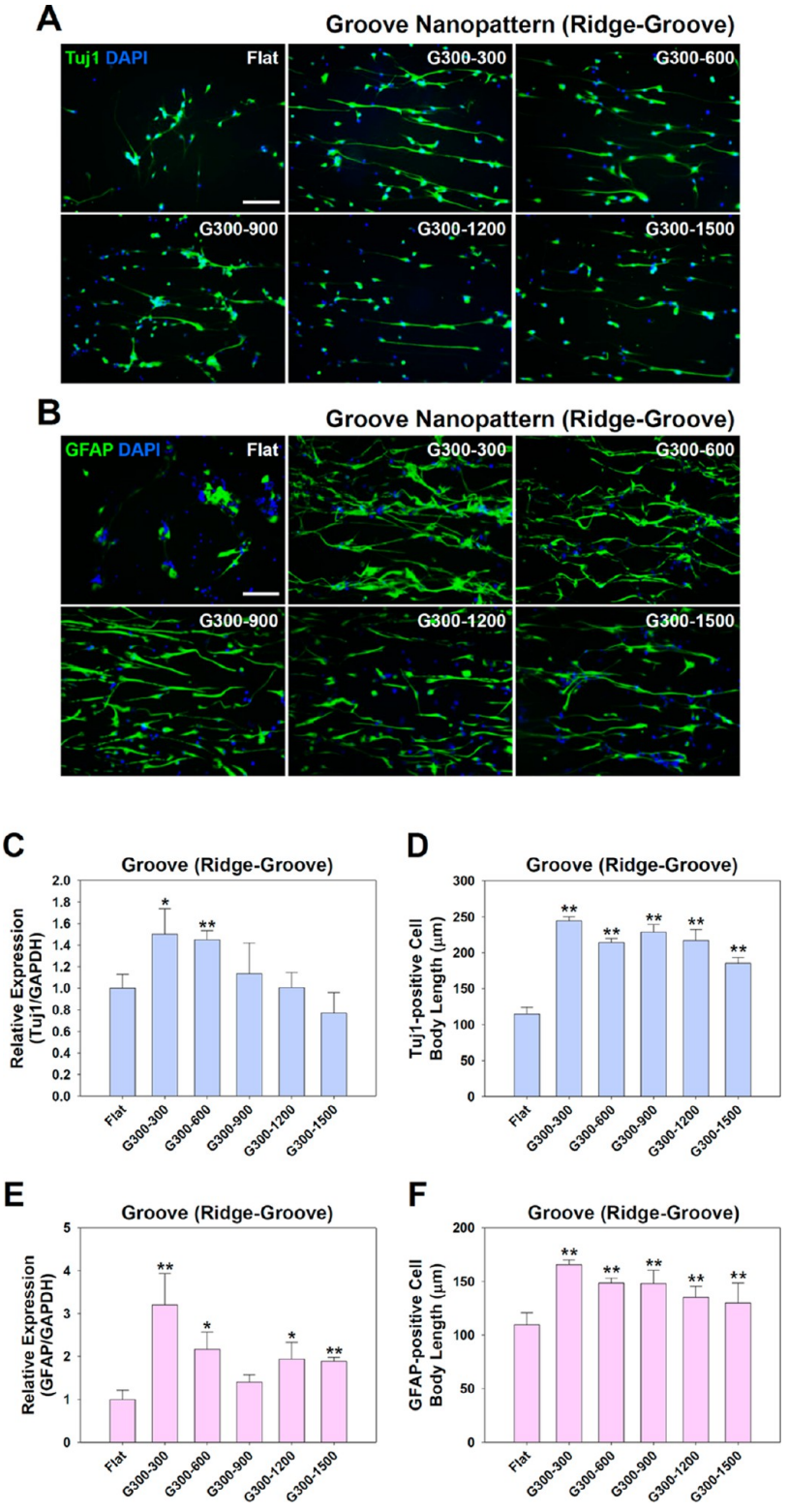

Figure 4. Enhanced differentiation of hNSCs occurred on groove nanopatterned substrates after 5 days in culture. Immunocytochemical staining was performed for the (A) neuronal marker Tuj1 and (B) astrocyte marker GFAP, scale bars = 100 μm. qRT-PCR was used to examine hNSC expression of (C) Tuj1 and (E) GFAP (n = 3, *p < 0.05, **p < 0.01, compared to the flat surface group). Body length was quantified in (D) Tuj1-positive cells and (F) GFAP-positive cells (n = 5, **p < 0.01, compared to the flat surface group).

hNSCs cultured on the grooved nanopatterned surfaces exhibited elongated morphology along the axis of the groove patterns (Figure 3A). hNSCs on the pillar nanopatterned surfaces showed radial alignment (Figure 3C). Finally, hNSCs cultured on the flat surfaces did not display aligned cell morphology (Figure 3A and C). Interestingly, nestin expression increased in hNSCs as the size of grooves and pillar gaps increased from 300 to 1500 nm. This was confirmed by qRT-PCR (Figure 3B and D) and may suggest that nanopatterned

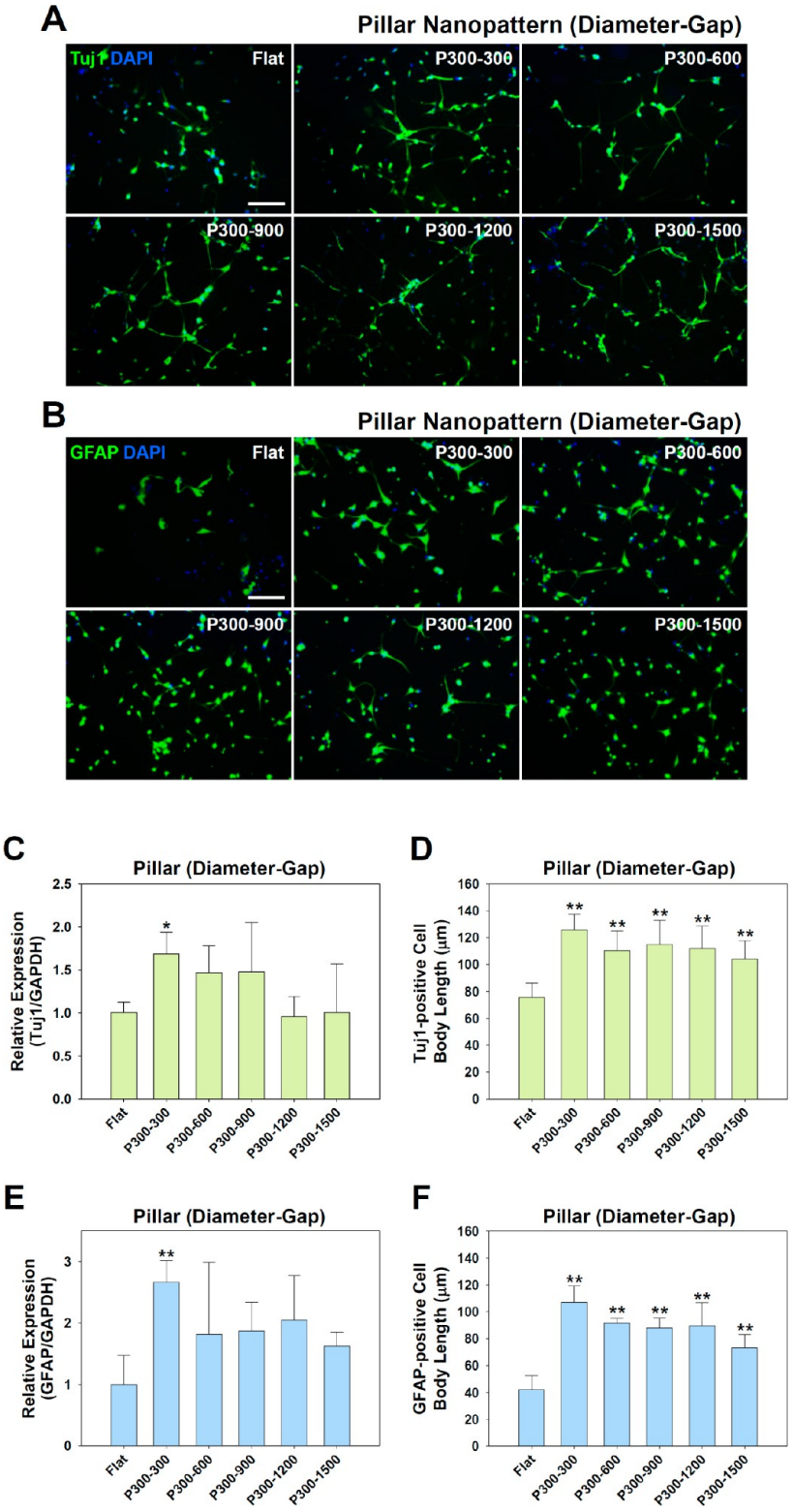

Figure 5. Enhanced differentiation of hNSCs occurred on pillar nanopatterned substrates after 5 days in culture. Immunocytochemical staining was performed for the (A) neuronal marker Tuj1 and (B) astrocyte marker GFAP, scale bars = 100 μm. qRT-PCR was used to examine hNSC expression of (C) Tuj1 and (E) GFAP (n = 3, *p < 0.05, **p < 0.01, compared to the flat surface group). Body length was quantified in (D) Tuj1-positive cells and (F) GFAP-positive cells (n = 5, **p < 0.01, compared to the flat surface group).

substrates with small grooves (G300−300 nm) or pillar gaps (P300−300 nm) accelerate hNSC differentiation.

3.3. Enhanced Differentiation of hNSCs on Nanopatterned Substrates. Neuronal and astrocyte differentiation of hNSCs was enhanced by the groove nanopatterned PUA substrates, and this enhancement was modulated by the dimension of the nanopatterned structures. Immunofluorescent staining for the neuronal marker Tuj1 revealed elongated

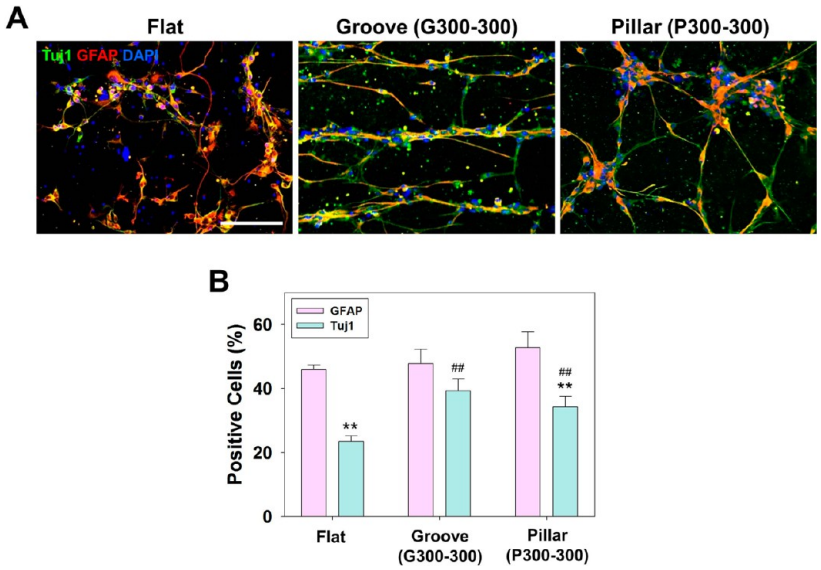

Figure 6. Altered differentiation propensity of hNSCs by nanopattern geometries after 5 days in culture. (A) Double immunofluorescent staining for neuronal marker Tuj1 and astrocyte marker GFAP, scale bar = 100 μm. (B) Relative proportion of Tuj1- or GFAP-positive cells (n = 3, $^{**}p < 0.01$, compared to proportion of GFAP-positive cells in each substrate group, $^{\#\#}p < 0.01$, compared to proportion of Tuj1-positive cells in flat substrate group).

neurite extension along the grooved nanopatterns (Figure 4A). qRT-PCR analysis showed that Tuj1 expression in hNSCs cultured on nanopatterns was inversely proportional to increases in groove size, from 300 to 1500 nm (Figure 4C). Tuj1 gene expression was upregulated in hNSCs grown on groove nanopatterned surfaces with small grooves (G300−300 nm and G300−600 nm) compared to those grown on flat surfaces and the nanopatterned surfaces with large grooves (G300−900 nm, G300−1200 nm, and G300−1500 nm) (Figure 4C). Immunofluorescent staining for the astrocyte marker GFAP revealed elongated GFAP-positive intermediate filaments extending from differentiated hNSCs on the groove nanopatterns (Figure 4B). hNSC GFAP gene expression was higher on the majority of groove nanopatterned surfaces compared to flat surfaces (Figure 4E). GFAP expression tended to decrease concomitantly as groove size increased from 300 to 1500 nm (Figure 4E). The lengths of Tuj1- and GFAP-positive cells were notably shorter in the flat substrate group than in the majority of the groove nanopatterned substrate groups (Figure 4D and F).

Neuron and astrocyte differentiation of hNSCs was enhanced on pillar nanopatterned substrates with specific dimensions. Immunofluorescent staining of Tuj1 showed radial alignment of neurites extending from differentiated hNSCs on pillar nanopatterns (Figure 5A). hNSCs cultured on pillar nanopatterns also exhibited radial alignment of GFAP-positive intermediate filaments (Figure 5B). Expression of Tuj1 and GFAP was much higher in hNSCs grown on nanopatterns with small pillar gaps (P300−300 nm) than on flat substrates or larger pillar nanopatterns (Figure 5C and E). These results were similar to the gene expression profiles of hNSCs on groove nanopatterns. Tuj1- or GFAP-positive cells were much longer when cultured on the majority of pillar nanopatterned surfaces compared to those on flat surfaces (Figure 5D and F).

Previous studies demonstrate that unidirectional patterns on culture substrates can induce neuronal differentiation.[14−16] In addition to pattern geometry, nanostructure dimensions also influence neuronal and glial differentiation of stem cells.[14,16,29,30] In these studies, stem cells displayed mature neuronal marker (Tuj1 and microtubule associated protein 2 (MAP2)) and astrocyte marker (GFAP) upregulation, as well as morphological changes to specific shapes and dimensions. Interestingly, a study by Yim et al. suggests that the size of patterned structures affects stem cell proliferation and differentiation.[14] They show that hMSC proliferation decreases and MAP2 expression increases as the width of groove patterns decreases from micrometers to nanometers (e.g., 10 μm, 1 μm, to 350 nm).[14] Our results also demonstrate that the geometry and dimension of surface topography can modulate neuronal and astrocyte differentiation of hNSCs (Figures 4 and 5). An explanation for this phenomenon may be that nanostructures with specific shapes and dimensions induce alignment and reorganization of the cytoskeleton in hNSCs, leading to activation of intracellular signal transduction and gene expression related to NSC differentiation.[8,9,14,31] While previous studies have predominately focused on comparing a single type of pattern shape and dimension, we examine the effect of nanopatterned structures with a variety of shapes and dimensions on hNSC differentiation.

Stem cell differentiation to lineages other than neuronal lineages has also been manipulated by nanopatterned substrates. Watari et al. demonstrated that nanoscale or submicrometer scale topography provided by ridge/groove patterns promotes osteogenic differentiation of hMSCs.[17] Interestingly, hMSC osteogenic differentiation was enhanced on groove nanopatterned substrates with a 400 nm pitch, compared to the planar controls and submicrometer patterned substrates with 1400 or 4000 nm pitches, as indicated by enhanced expression of osteogenic markers, RUNX2 and BGLAP, and calcium deposition.[17] It appears that the differentiation propensity of hMSCs according to pattern size is similar to that of the hNSC differentiation observed in our study. In fact, a recent study demonstrated that collagen I-coated hydrogel substrates with small pore sizes increase adhesive cell area and promote osteogenic differentiation of hMSCs.[4] Substrates with other types of geometries, including

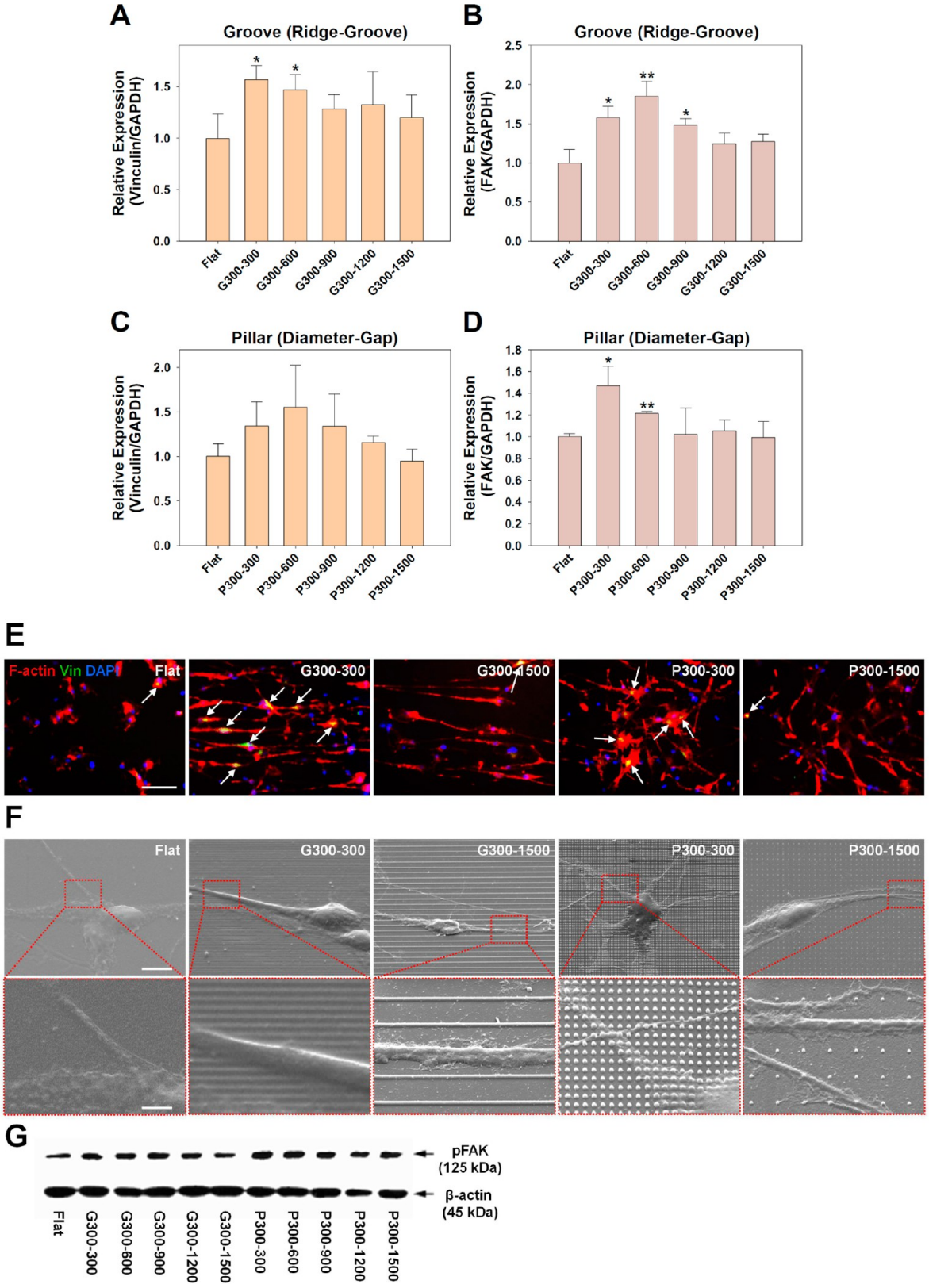

Figure 7. Focal adhesion formation in hNSCs is regulated according to the size of nanopatterns (after 5 days in culture). qRT-PCR was used to examine expression of focal adhesion genes (A, C) vinculin and (B, D) FAK in hNSCs grown on groove and pillar nanopatterned substrates ($n = 3$, $^{*}p < 0.05$, $^{**}p < 0.01$, compared to the flat surface group). (E) Cytoskeletal (F-actin; red) and focal adhesion proteins (vinculin; yellow) were costained in hNSCs on flat and nanopatterned substrates (groove 300−300 nm, groove 300−1500 nm, pillar 300−300 nm, and pillar 300−1500 nm), scale bar = 50 μm. The arrows indicate vinculin-positive focal contact points in hNSCs. (F) SEM images were obtained of hNSCs on flat and nanopatterned substrates (groove 300−300 nm, groove 300−1500 nm, pillar 300−300 nm, and pillar 300−1500 nm), scale bars = 10 μm (top row) and 2 μm (bottom row). (G) Western blot was used to examine expression of phosphorylated FAK in hNSCs on flat and nanopatterned substrates.

nanopits and nanotubes, have also been shown to enhance osteogenic differentiation of hMSCs by stimulating the bone morphogenetic protein pathway.[8,32]

Many studies employ a combination of topographical cues and soluble factors to create synergistic effects that promote stem cell commitment to a specific lineage of interest. For example, Yim et al. used a biochemical reagent (retinoic acid) to promote neuronal differentiation of hMSCs cultured on nanopatterned substrates.[14] Another study performed by Watari et al. also used differentiation medium containing osteogenesis-inducing soluble factors for osteogenic differentiation of hMSCs on patterned substrates.[17] Although combined topographical and biochemical cues may further enhance lineage differentiation of stem cells, the combination makes it difficult to interpret the effect of topography alone on stem cell differentiation. For this reason, we did not use soluble factors to guide hNSC lineage specification in our experiments on nanopatterned substrates.

3.4. Altered Differentiation Propensity of hNSCs by Nanopattern Geometries. Next, we examined the effects of nanopattern geometries on lineage specification of differentiated hNSCs. The cells on three types of substrates (flat, groove 300−300, and pillar 300−300) were double immunofluorescently stained for Tuj1 (neuronal marker) and GFAP (astrocyte marker) to confirm which geometric nanopattern favors neuronal and glial differentiation, respectively (Figure 6A). To quantify the relative proportion of cells expressing Tuj1 or GFAP, we counted the number of Tuj1- or GFAP-positive cells in the images of double immunofluorescent staining for Tuj1 and GFAP and calculated the percentage ratio of each cell type to total cell population (DAPI-positive cells) (Figure 6B).

The quantification result from double immunofluorescent staining for Tuj1 and GFAP reveals that nanopattern geometries can alter lineage specification of hNSCs. Given that the proportion of GFAP-positive cells was generally higher than that of Tuj1-positive cells (Figure 6B), glial differentiation to astrocytes seems to be more dominant in hNSCs on three tested substrates (flat, G300−300, and P300−300) than neuronal differentiation. Interestingly, the use of groove nanopatterns increased the proportion of Tuj1-positive cells compared with pillar nanopatterns (Figure 6B), indicating enhanced neuronal differentiation of hNSCs by anisotropic groove nanopatterns. There was no significant alteration in hNSC differentiation propensity depending on nanopattern sizes (data not shown).

Several studies have described that shapes and dimensions of topographical features modulate differentiation propensity of stem cells. Moe et al. reported that nano- and microscale anisotropic patterns (250 nm grafting, 2 μm grafting) enhance neuronal differentiation of neural progenitor cells (NPCs) while isotropic patterns (1 μm pillar, 2 μm hole) promote glial differentiation of NPCs.[29] The study reported by Ankam et al. also reported similar observation in differentiation propensity of hESCs to neuronal or glial lineage, which is dependent on shapes and sizes of substrate topography.[30]

Considering the role of nanopattern geometries on hNSC lineage specification, the choice of specific nanopatterns would be critical for therapeutic applications. Since anisotropic groove nanopatterned substrate can enhance neuronal differentiation and neurite extension of hNSCs along the patterned lines (Figure 4A), this type of nanopattern may be more advantageous for stem cell therapy to regenerate axons with elongated, extended neurites in longitudinal direction. Isotropic pillar nanopattern may be more appropriate to regenerate highly branched neural networks or dendrites with glial cells because it can promote astrocyte differentiation as well as radial neurite extension of hNSCs (Figures 5A and Figure 6).

3.5. Regulation of hNSC Focal Adhesion by Nanopatterned Structures. We examined whether nanopatterned substrates can modulate hNSC focal adhesion to enhance differentiation. qRT-PCR analysis revealed that vinculin expression, a representative focal adhesion protein, was much higher in hNSCs grown on the majority of groove and pillar nanopatterned substrates, especially those with smaller grooves (G300−300 and G300−600 nm) and pillar gap (P300−600 nm), compared to those grown on flat substrates (Figure 7A and C). Expression of FAK, another important protein involved in focal adhesion complex formation, was also significantly enhanced in hNSCs cultured on nanopatterns with smaller grooves (G300−300 and G300−600 nm) and pillar gaps (P300−300 and P300−600 nm) compared to the flat substrates (Figure 7B and D). In general, hNSC expression of vinculin and FAK decreased on patterns with large grooves (G300−1200 and G300−1500 nm) or pillar gaps (P300−1200 and P300−1500 nm) (Figure 7A−D). These results may indicate that substrates with submicrometer scale groove and pillar patterns (1200, 1500 nm) are less effective at promoting focal adhesion complex development in hNSCs than nanoscale-patterned substrates with grooves or pillar gaps below 600 nm.

Costaining of cytoskeletal (F-actin) and focal adhesion (vinculin) proteins supported that focal adhesion formation in hNSCs (indicated by vinculin staining) was enhanced on nanopatterned surfaces with smaller grooves and pillar gaps (300−300 nm) compared to those on flat surfaces or surfaces with larger grooves and pillar patterns (300−1500 nm; Figure 7E). Alignment and reorganization of the F-actin filament, observed by phalloidin staining, was further facilitated on nanopatterns with 300−300 nm dimensions (Figure 7E). SEM analysis demonstrated that nanopatterned substrates with small grooves and pillar gaps (300−300 nm) may provide more contact points that facilitate hNSC focal adhesion formation than those on flat substrates or substrates with 300−1500 nm dimensions (Figure 7F). Western blot analysis revealed that phosphorylated FAK, an activated form of FAK in the focal adhesion signaling pathway, was upregulated in hNSCs cultured on nanopatterned surfaces with grooves and pillars at 300−300 and 300−600 nm dimensions compared to those on flat surfaces and surfaces with grooves and pillar patterns with 300−1200 and 300−1500 nm dimensions (Figure 7G). This result suggests that the FAK signaling pathway in hNSCs can be stimulated by nanoscale patterned arrays (300−300 and 300−600 nm).

Extracellular nanotopography of specific shape and dimension may facilitate focal adhesion protein assembly and cytoskeleton reorganization in cells.[33] Cell adhesion to the ECM is mediated by specific cell surface receptors called integrins (e.g., fibronectin to the $\alpha5\beta1$ integrin).[18,34] When integrins are activated by binding to nanoscale ECM structures on the surface of patterned substrates, additional integrins cluster around the activated sites and FAK and other adapter proteins such as vinculin and paxillin are recruited to the integrin clusters.[9] This results in the formation of focal adhesion complexes that respond to ECM surface topography.[9] Because the focal adhesion complex links ECM to the contractile cytoskeleton, rearrangement of focal adhesions

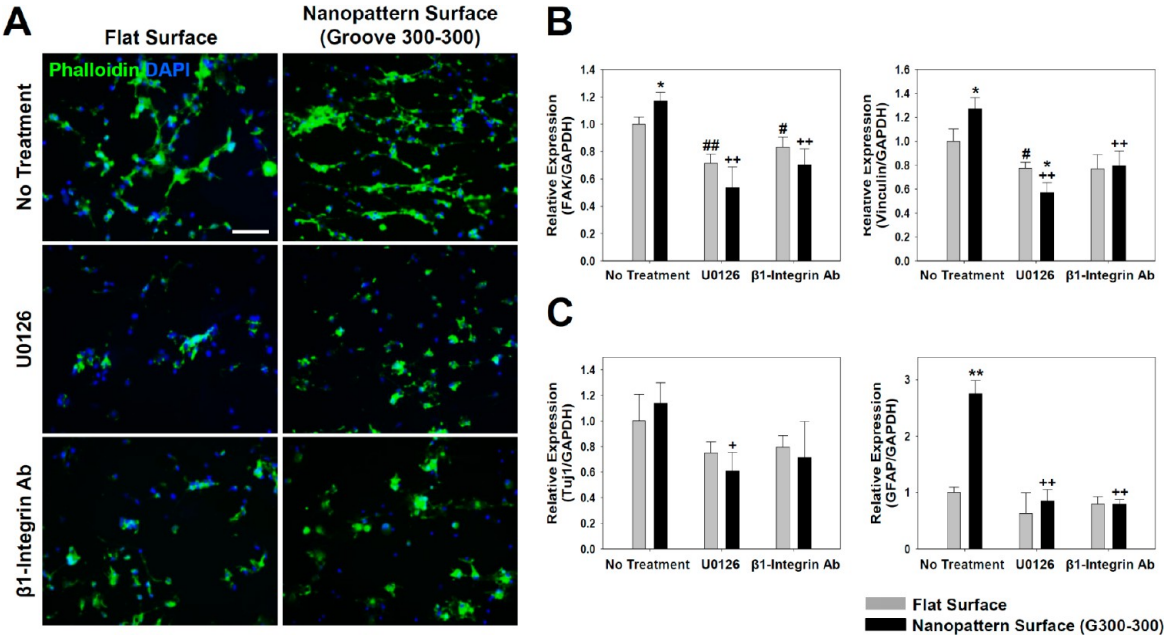

Figure 8. Inhibition of adhesion, alignment, and differentiation was achieved in hNSCs by blocking the integrin-mediated focal-adhesion-signaling pathway (after 1 day in culture). (A) The cytoskeleton (F-actin) of hNSCs treated with U0126 (MEK-ERK pathway inhibitor) and antibodies against integrin β1 was stained with phalloidin, scale bar = 100 μm. Cell nuclei were stained with DAPI. qRT-PCR was used to examine gene expression of (B) focal adhesion proteins (FAK and vinculin) and (C) differentiation markers Tuj1 and GFAP in hNSCs treated with U0126 and anti-integrin β1 and in untreated hNSCs ($^{*}p < 0.05$ vs each flat group, $\#p < 0.05$, and $\#\#p < 0.01$ vs no treated flat group, $^{+}p < 0.05$ and $^{++}p < 0.01$ vs no treated nanopattern group).

induced by surface topography reorganizes cytoskeletal components such as F-actin, which alters mechanical tension in the cells. Thus, mechanical stimulation can be propagated by the focal adhesion complex to activate focal adhesion signaling pathways such as FAK phosphorylation, as shown in Figure 7G. In this study, we also found that reorganization of the focal adhesion−cytoskeleton complex occurs according to the size and geometry of the nanopatterned structures coated with fibronectin (Figure 7E). Our results show that enhanced focal adhesion formation occurs in hNSCs on patterns with small nanostructures. This is consistent with findings from a previous study that show reduced focal adhesion of hMSCs on RGD peptide-coated groove nanopatterns with increased gaps.[35] In other words, the ability of stem cells to form mature focal adhesions may be reduced on patterned substrates with increased lateral spacing.[35]

As mentioned previously, the rearrangement of focal adhesions and the cytoskeleton in response to ECM surface topography can alter nucleus organization and consequently influence gene expression profiles in cells.[8] Cytoskeletal reorganization causes changes to cell morphology. These changes cause mechanical tension to be transferred to the nucleus through reorganized actin filaments, which can rearrange the centromere by deformation of the nucleus.[20,36] This ultimately alters gene expression related to stem cell differentiation.[14,31,36] As a result, this type of mechanosensitive transduction may be an important pathway that determines stem cell function and phenotype. Therefore, topographical manipulation of stem cell focal adhesions is expected to enhance differentiation into specific lineages by activating mechanosensitive intracellular signaling pathways.[8,37] In support of this concept, Yu et al. reported that micropattern arrays modulate myogenic differentiation of hMSCs through focal adhesion regulation.[38]

Several stusdies have employed similar sizes of nanopatterned substrates to ours for promoting focal adhesion formation and neuronal differentiation of stem cells. Teo et al. reported that nanotopography with 250 nm line patterns enhances neuronal differentiation of hMSCs through FAK activation.[39] It was also reported that the culture of stem cells on nanopatterned surfaces with 350-nm groove/ridge promotes neuronal differentiation of hESCs and hMSCs compared with flat or micropatterned surfaces.[14,15] These results are consistent with the findings from our study demonstrating that nanopatterns with small size groove and pillar (300−300 nm) are more effective for developing focal adhesion formation in hNSCs and facilitating differentiation of hNSCs (Figures 4, 5, and 7).

One of potential future studies would be comparison of stem cell behavior on the substrates with nanotopographical features and the substrates produced by microcontact printing. Several studies have reported microcontact printing technique to produce the substrates with the patterns of ECM proteins and cell−cell signaling ligands on nonadhesive background surface for stem cell engineering.[40,41] These studies demonstrated that ECM, adhesion molecule, and cell signaling ligand printed patterns on the substrates modulate spatial differentiation of NSCs even though these patterns do not provide topographical cues for enhanced focal adhesion formation in stem cells. Considering that microcontact printing technology can provide a valuable tool for investigating stem cell−biomaterial interfaces, comparison studies would be interesting to examine whether hNSC differentiation on the substrates produced by microcontact printing is similar to that on nanopatterned substrates employed in our study.

3.6. Mechanism of Nanotopographical Stimulation for Enhanced hNSC Differentiation. Last, we investigated the mechanism of nanotopographical-enhanced hNSC differ-

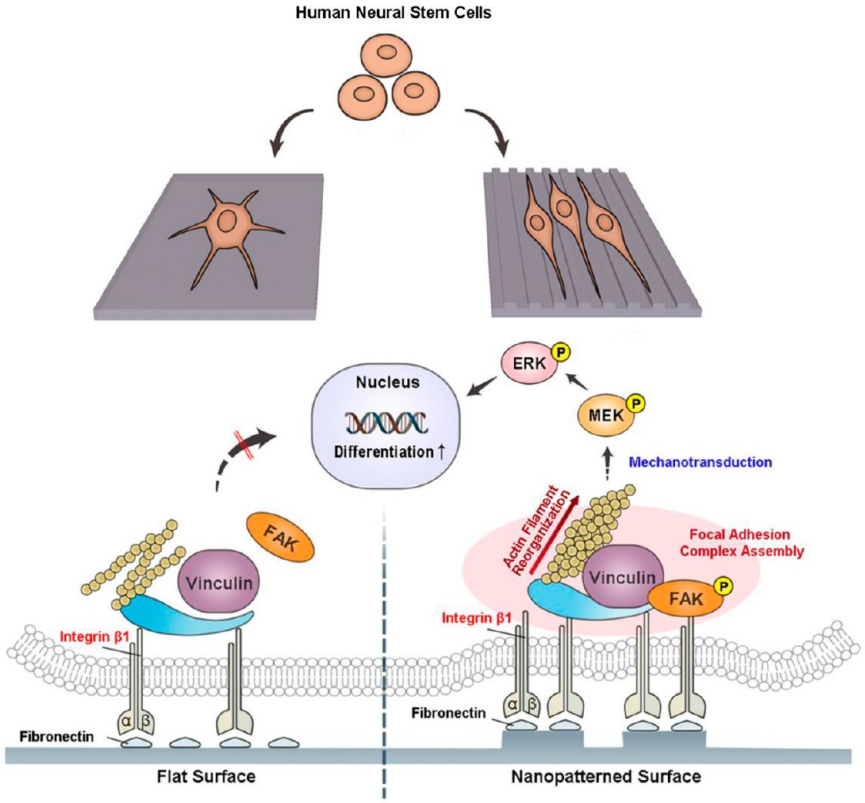

Figure 9. Potential mechanism for nanotopographical manipulation of the focal adhesion signaling pathway and differentiation of hNSCs is depicted.

entiation. In this study, we used the ECM protein fibronectin to coat the nanopatterned substrates for hNSC adhesion and differentiation. Because ECM proteins can activate integrin-dependent signaling pathways leading to tyrosine phosphorylation of FAK,[42,43] we focused on integrin-mediated binding of hNSCs to fibronectin as an initial point of activation for the focal adhesion signaling pathway. We also examined the MEK/ERK pathway as a downstream intracellular signaling pathway to mechanosensitive FAK phosphorylation because this pathway is involved in neurite outgrowth during stem cell differentiation.[42,44]

Inhibition of the integrin-mediated intracellular signaling pathway diminished the effects of nanopatterned topography on enhancement of hNSC focal adhesion and differentiation. Adhesion of hNSCs to the fibronectin-coated nanopatterned substrates was completely abolished using antibodies against integrin β1, an integrin that mediates cell binding to fibronectin (Figure 8A).[42] Blocking integrin-mediated binding of hNSCs inhibited hNSC alignment along the nanopatterned topography (Figure 8A). We also blocked the MEK-ERK pathway, one of the mechanosensitive intracellular signaling pathways related to NSC differentiation.[42] Treatment with an inhibitor (U0126) of the MEK-ERK pathway led to significant inhibition in hNSC adhesion, spreading, and neurite outgrowth (Figure 8A). hNSCs treated with integrin β1antibodies and U0126 exhibited small circular cluster morphology, whereas hNSCs in the untreated control group adhered well to the substrates and displayed extended and aligned morphology on the groove-patterned substrates (Figure 8A). FAK and vinculin expression in hNSCs was significantly reduced by treatment with integrin β1antibodies and U0126 compared to the no treatment group (Figure 8B). Decreased expression of these proteins was more evident in the nanopatterned substrate group than in the flat substrate group. This indicates the significance of nanotopographical stimulation to focal adhesion formation.

Nanotopography-enhanced hNSC differentiation was reversed by treatment with integrin β1 antibodies and U0126, as indicated by qRT-PCR analysis of Tuj1 and GFAP (Figure 8C). This means that inhibition of hNSC adhesion and decreased expression of focal adhesion proteins impaired the activation of mechanosensitive intracellular signal transduction that promotes stem cell differentiation. Our results suggest that integrin-β1-mediated binding of hNSCs to fibronectin on nanopatterned substrates facilitates focal adhesion formation and FAK phosphorylation, and subsequently activates the MEK/ERK signaling pathway (Figure 9). This activation of the MEK/ERK pathway may ultimately enhance hNSC differentiation to neurons or astrocytes even without supplementation with growth factors or lineage specification reagents (Figure 9).[42]

4. CONCLUSIONS

In summary, our study demonstrates that nanotopographical cues manipulate focal adhesion and differentiation of hNSCs. We identified the optimal scale of surface nanostructures to promote hNSC differentiation by showing that nanopatterns of biomimetic sizes (scale of 300−600 nm) enhanced neuronal and astrocyte differentiation. Our results indicate that nanoscale patterns alone can effectively induce differentiation of hNSCs into neuronal and astrocyte lineages without addition of biochemical or biological agents. We also elucidated the underlying mechanisms for how these biomechanical cues influence hNSC differentiation. Future functional assessment of synaptic transmission and electrophysiological properties of the differentiated hNSCs will be of great interest. Our results can provide insights into developing culture substrates and tissue

engineering scaffolds that improve the efficacy of stem cell therapeutics.

AUTHOR INFORMATION

Corresponding Author

*(Prof. Seung-Woo Cho) Mailing address: Department of Biotechnology, Yonsei University, 50 Yonsei-ro, Seodaemun-gu, Seoul 120-749, Republic of Korea. Tel.: +82-2-2123-5662. Fax: +82-2-362-7265. E-mail: seungwoocho@yonsei.ac.kr. (Dr. Jinseok Kim) Mailing address: Center for Bionics, Korea Institute of Science and Technology, 39-1 Hawolgok-dong, Seongbuk-gu, Seoul 136-791, Republic of Korea. Tel.: +82-2-958-6745. Fax: +82-2-958-6446. E-mail: jinseok@kist.re.kr.

Notes

The authors declare no competing financial interest.

ACKNOWLEDGMENTS

This work was supported by grants (2010-0020409, 2010-0022037, and 2010-0020289) from the National Research Foundation of Korea (NRF) and Healthcare Technology R&D Project (A091159), Republic of Korea. This work was also supported by NRF grant funded by the Korean Government (NRF-2013-Fostering Core Leaders of the Future Basic Science Program). This work was partially supported by Korea Institute of Science and Technology (KIST) Institutional Program (2E24057).

REFERENCES

(1) Teo, B. K.; Ankam, S.; Chan, L. Y.; Yim, E. K. *Methods Cell Biol.* **2010**, *98*, 241−294.
(2) Guilak, F.; Cohen, D. M.; Estes, B. T.; Gimble, J. M.; Liedtke, W.; Chen, C. S. *Cell Stem Cell* **2009**, *5*, 17−26.
(3) Engler, A. J.; Sen, S.; Sweeney, H. L.; Discher, D. E. *Cell* **2006**, *126*, 677−689.
(4) Trappmann, B.; Gautrot, J. E.; Connelly, J. T.; Strange, D. G.; Li, Y.; Oyen, M. L.; Cohen Stuart, M. A.; Boehm, H.; Li, B.; Vogel, V.; Spatz, J. P.; Watt, F. M.; Huck, W. T. *Nat. Mater.* **2012**, *11*, 642−649.
(5) Yang, Y.; Kulangara, K.; Lam, R. T.; Dharmawan, R.; Leong, K. W. *ACS Nano* **2012**, *6*, 8591−8598.
(6) Choi, Y. S.; Vincent, L. G.; Lee, A. R.; Dobke, M. K.; Engler, A. J. *Biomaterials* **2012**, *33*, 2482−2491.
(7) Kulangara, K.; Yang, Y.; Yang, J.; Leong, K. W. *Biomaterials* **2012**, *33*, 4998−5003.
(8) Dalby, M. J.; Gadegaard, N.; Tare, R.; Andar, A.; Riehle, M. O.; Herzyk, P.; Wilkinson, C. D.; Oreffo, R. O. *Nat. Mater.* **2007**, *6*, 997−1003.
(9) Yim, E. K.; Darling, E. M.; Kulangara, K.; Guilak, F.; Leong, K. W. *Biomaterials* **2010**, *31*, 1299−1306.
(10) Chen, W.; Villa-Diaz, L. G.; Sun, Y.; Weng, S.; Kim, J. K.; Lam, R. H.; Han, L.; Fan, R.; Krebsbach, P. H.; Fu, J. *ACS Nano* **2012**, *6*, 4094−4103.
(11) Chan, L. Y.; Birch, W. R.; Yim, E. K.; Choo, A. B. *Biomaterials* **2013**, *34*, 382−392.
(12) McMurray, R. J.; Gadegaard, N.; Tsimbouri, P. M.; Burgess, K. V.; McNamara, L. E.; Tare, R.; Murawski, K.; Kingham, E.; Oreffo, R. O.; Dalby, M. J. *Nat. Mater.* **2011**, *10*, 637−644.
(13) Jeon, K.; Oh, H. J.; Lim, H.; Kim, J. H.; Lee, D. H.; Lee, E. R.; Park, B. H.; Cho, S. G. *Biomaterials* **2012**, *33*, 5206−5220.
(14) Yim, E. K.; Pang, S. W.; Leong, K. W. *Exp. Cell Res.* **2007**, *313*, 1820−1829.
(15) Lee, M. R.; Kwon, K. W.; Jung, H.; Kim, H. N.; Suh, K. Y.; Kim, K.; Kim, K. S. *Biomaterials* **2010**, *31*, 4360−4366.
(16) Béduer, A.; Vieu, C.; Arnauduc, F.; Sol, J. C.; Loubinoux, I.; Vaysse, L. *Biomaterials* **2012**, *33*, 504−514.
(17) Watari, S.; Hayashi, K.; Wood, J. A.; Russell, P.; Nealey, P. F.; Murphy, C. J.; Genetos, D. C. *Biomaterials* **2012**, *33*, 128−136.
(18) Seo, C. H.; Furukawa, K.; Montagne, K.; Jeong, H.; Ushida, T. *Biomaterials* **2011**, *32*, 9568−9575.
(19) Seo, C. H.; Jeong, H.; Furukawa, K. S.; Suzuki, Y.; Ushida, T. *Biomaterials* **2013**, *34*, 1764−1771.
(20) Chalut, K. J.; Kulangara, K.; Giacomelli, M. G.; Wax, A.; Leong, K. W. *Soft Matter* **2010**, *6*, 1675−1681.
(21) Pan, Z.; Yan, C.; Peng, R.; Zhao, Y.; He, Y.; Ding, J. *Biomaterials* **2012**, *33*, 1730−1735.
(22) Temple, S. *Nature* **2001**, *414*, 112−117.
(23) Chojnacki, A.; Weiss, S. *Nat. Protoc.* **2008**, *3*, 935−940.
(24) Yang, K.; Lee, J. S.; Kim, J.; Lee, Y. B.; Shin, H.; Um, S. H.; Kim, J. B.; Park, K. I.; Lee, H.; Cho, S. W. *Biomaterials* **2012**, *33*, 6952−6964.
(25) Cho, S. W.; Goldberg, M.; Son, S. M.; Xu, Q.; Yang, F.; Mei, Y.; Bogatyrev, S.; Langer, R.; Anderson, D. G. *Adv. Funct. Mater.* **2009**, *19*, 3112−3118.
(26) Park, H. J.; Lee, J.; Kim, M. J.; Kang, T. J.; Jeong, Y.; Um, S. H.; Cho, S. W. *Biomaterials* **2012**, *33*, 9148−9156.
(27) Kim, J. Y.; Park, K. S.; Kim, Z. S.; Baek, K. H.; Do, L. M. *Soft Matter* **2012**, *8*, 1184−1189.
(28) Kim, M. J.; Lee, B.; Yang, K.; Park, J.; Jeon, S.; Um, S. H.; Kim, D. I.; Im, S. G.; Cho, S. W. *Biomaterials* **2013**, *34*, 7236−7246.
(29) Moe, A. A.; Suryana, M.; Marcy, G.; Lim, S. K.; Ankam, S.; Goh, J. Z.; Jin, J.; Teo, B. K.; Law, J. B.; Low, H. Y.; Goh, E. L.; Sheetz, M. P.; Yim, E. K. *Small* **2012**, *8*, 3050−3061.
(30) Ankam, S.; Suryana, M.; Chan, L. Y.; Moe, A. A.; Teo, B. K.; Law, J. B.; Sheetz, M. P.; Low, H. Y.; Yim, E. K. *Acta Biomater.* **2013**, *9*, 4535−4545.
(31) Dalby, M. J.; Riehle, M. O.; Yarwood, S. J.; Wilkinson, C. D.; Curtis, A. S. *Exp. Cell Res.* **2003**, *284*, 274−282.
(32) Oh, S.; Brammer, K. S.; Li, Y. S.; Teng, D.; Engler, A. J.; Chien, S.; Jin, S. *Proc. Natl. Acad. Sci. U.S.A.* **2009**, *106*, 2130−2135.
(33) Pennisi, C. P.; Dolatshahi-Pirouz, A.; Foss, M.; Chevallier, J.; Fink, T.; Zachar, V.; Besenbacher, F.; Yoshida, K. *Colloids Surf., B* **2011**, *85*, 189−197.
(34) Wojcik-Stanaszek, L.; Gregor, A.; Zalewska, T. *Acta Neurobiol. Exp.* **2011**, *71*, 103−112.
(35) Frith, J. E.; Mills, R. J.; Cooper-White, J. J. *J. Cell Sci.* **2012**, *125*, 317−327.
(36) Maniotis, A. J.; Chen, C. S.; Ingber, D. E. *Proc. Natl. Acad. Sci. U.S.A.* **1997**, *94*, 849−854.
(37) Yang, Y.; Leong, K. W. *Wiley Interdiscip. Rev.: Nanomed. Nanobiotechnol.* **2010**, *2*, 478−495.
(38) Yu, H.; Tay, C. Y.; Pal, M.; Leong, W. S.; Li, H.; Li, H.; Wen, F.; Leong, D. T.; Tan, L. P. *Adv. Healthcare Mater.* **2013**, *2*, 442−449.
(39) Teo, B. K.; Wong, S. T.; Lim, C. K.; Kung, T. Y.; Yap, C. H.; Ramagopal, Y.; Romer, L. H.; Yim, E. K. *ACS Nano* **2013**, *7*, 4785−4798.
(40) Ruiz, A.; Zychowicz, M.; Ceriotti, L.; Mehn, D.; Sirghi, L.; Rauscher, H.; Mannelli, I.; Colpo, P.; Buzanska, L.; Rossi, F. *Biomed. Microdevices* **2013**, *15*, 495−507.
(41) Wang, Y.; Xu, Z.; Kam, L. C.; Shi, P. *Adv. Healthcare Mater.* **2013**, DOI: 10.1002/adhm.201300082.
(42) Chen, Y. C.; Lee, D. C.; Tsai, T. Y.; Hsiao, C. Y.; Liu, J. W.; Kao, C. Y.; Lin, H. K.; Chen, H. C.; Palathinkal, T. J.; Pong, W. F.; Tai, N. H.; Lin, I. N.; Chiu, I. M. *Biomaterials* **2010**, *31*, 5575−5587.
(43) Ivankovic-Dikic, I.; Gronroos, E.; Blaukat, A.; Barth, B. U.; Dikic, I. *Nat. Cell Biol.* **2000**, *2*, 574−581.
(44) Mruthyunjaya, S.; Manchanda, R.; Godbole, R.; Pujari, R.; Shiras, A.; Shastry, P. *Biochem. Biophys. Res. Commun.* **2010**, *391*, 43−48.